Chemical Science

ROYAL SOCIETY OF CHEMISTRY

EDGE ARTICLE

View Article Online
View Journal | View Issue

Open Access Article. Published on 04 April 2025. Downloaded on 6/15/2025 9:25:23 PM.
This article is licensed under a Creative Commons Attribution-NonCommercial 3.0 Unported Licence.

Check for updates

Cite this: *Chem. Sci.*, 2025, **16**, 8470

All publication charges for this article have been paid for by the Royal Society of Chemistry

Electric-field-induced covalent condensation of boronic acids in water microdroplets†

Yue-Wen Zhou,‡ Ming-Yang Jia,‡ Jun-Lei Yang, Qinlei Liu * and Zhen-Feng Cai *

Received 24th February 2025
Accepted 2nd April 2025

DOI: 10.1039/d5sc01466b

rsc.li/chemical-science

The influence of electric fields (EFs) on chemical reactions has attracted significant interest due to their ability to modulate reaction rates, pathways, and selectivity. Although EFs have been experimentally demonstrated to facilitate various reactions, clear evidence for their role in covalent condensation has remained limited. Herein, we provide experimental evidence of electric-field-induced covalent condensation of boronic acids, utilizing the strong EFs at the air–liquid interface of microdroplets to induce the reaction. Microdroplet-based chemistry provides interfacial electric field intensities as high as *ca.* 10^9 V m^{-1}, offering a robust platform for the systematic investigation of boronate linkage formation and subsequent condensation of boronic acids. Our results confirm the role of EFs in facilitating the room-temperature condensation of boronic acids, providing direct insights into the electric-field-induced polymerization process and presenting an experimental approach for investigating these processes in solution.

Introduction

Electric fields (EFs) have been recognized as a powerful tool for manipulating chemical reactions, enabling precise control over reaction pathways and selectivity.[1–5] By reorganizing the electron distribution of molecules, EFs can stabilize or destabilize charge-separated intermediates, and lower the activation barriers of the electron transfer process, thus catalyzing chemical reactions electrostatically. Theoretically, the catalytic effects of EFs have been explored by advanced *ab initio* molecular dynamics (AIMD) and path-integral AIMD simulations and it has been revealed that EFs are capable of accelerating chemical reactions within liquids.[2,5–7] In these simulations, EFs drastically lower activation barriers and reshape reaction pathways, enabling spontaneous transformations such as the methanol dehydration reaction and ethanol dehydrogenation reaction.[8–10] Experimentally, it has also been demonstrated that EFs can facilitate a range of chemical processes, including the Menshutkin reaction,[11] Ullmann coupling reactions,[12] homolytic cleavage of O–O bonds,[13] and alkyl-transfer reactions.[14] These studies have shown the potential of EFs to not only accelerate known reaction pathways, but also induce novel reaction mechanisms.

The covalent condensation of boronic acids is an important reaction for constructing extended polymeric networks, including two-dimensional polymeric materials such as covalent organic frameworks (COFs).[15–19] Developing novel methods to drive such polymerization reactions is crucial for advancing material synthesis and tailoring material properties.[20–22] It has been suggested that highly localized EFs generated by scanning tunneling microscopy (STM) can reversibly induce room-temperature polymerization and depolymerization of boronic acids on solid surfaces.[4] However, considering that the STM tip can also potentially act as a powerful oxidizing or reducing agent,[23] direct experimental evidence of this electric-field-induced condensation is still lacking. Thus, it is important to separate the tip effects and obtain clearer experimental insights into the EF-induced polymerization of boronic acids.

Microdroplet-based chemistry has emerged as a novel platform for studying reaction dynamics under unique physical conditions, including the presence of strong interfacial EFs.[11,24–26] One of the most notable features of microdroplets is the spontaneous generation of a strong electric field at the air–water interface. This may result from the formation of double electric layers due to charge separation at the air–water interface, the spontaneous alignment of water molecules, or partial charge transfer between water molecules.[27–29] Recently, several studies have reported that the electric field may have a very subtle catalytic effect on the Diels–Alder reaction, and that the solid–water interface also plays a crucial role in microdroplet reactions, making the contribution of the air–water interface

Key Laboratory of Green Chemistry and Technology of Ministry of Education, College of Chemistry, Sichuan University, 29 Wangjiang Road, Chengdu 610064, P. R. China. E-mail: liuqinlei@scu.edu.cn; caizf@scu.edu.cn

† Electronic supplementary information (ESI) available: MS^2 spectra of different products; mass spectrum of BDBA in microdroplets; transition states of the BPBA dimer; potential energy profile of PBA condensation; Mulliken charge and bond length of the TS. See DOI: https://doi.org/10.1039/d5sc01466b

‡ These authors contributed equally to this work.

© 2025 The Author(s). Published by the Royal Society of Chemistry

Open Access Article. Published on 04 April 2025. Downloaded on 6/15/2025 9:25:23 PM. This article is licensed under a Creative Commons Attribution-NonCommercial 3.0 Unported Licence.

elusive.[30,31] However, the unique importance of the air–water interface in microdroplets has been further demonstrated and affirmed through levitated droplet technology and electrochemical methods.[32,33] Experimental and theoretical studies have shown that the EFs at the interface of microdroplets can reach intensities comparable to those generated by STM tips (*ca.* 10^9 V m^{-1}), providing a solution-phase environment where electric-field-induced reactions can be directly observed.[29,34–36] Therefore, the strong EFs present at the microdroplet interface present an ideal platform to study the condensation of boronic acids, potentially providing direct mechanistic insights that are difficult to capture with STM techniques.

In this work, we provide experimental evidence of electric-field-induced covalent condensation of boronic acids, using the strong EFs at the microdroplet interface to drive the reaction. By systematically investigating the reaction process in this unique environment, we reveal the role of EFs in facilitating the self-condensation and co-condensation of boronic acids. Our findings not only confirm the hypothesized role of EFs in boronic acid condensation but also offer a new experimental approach for studying electric-field-induced reactions in solution. This work advances the understanding of electric-field effects on polymerization and lays the foundation for the controlled synthesis of boron-based materials and other covalent organic frameworks at room temperature under ambient conditions.

Methods

Chemicals and sample preparation

Phenylboronic acid (PBA, 97%) was purchased from Beijing InnoChem Technology Co., Ltd. 1,4-Benzenediboronic acid (BDBA, 98%) and 4,4′-biphenyldiboronic acid (BPBA, 98%) were purchased from Shanghai Aladdin Biochemical Technology Co., Ltd. Pure water (HPLC grade) was purchased from Alfa Aesar China Chemical Co., Ltd and MeOH (HPLC grade) was purchased from Sigma-Aldrich. A solution of pure water (HPLC grade) and MeOH (1 : 4 by volume) was prepared for use in the experiments. Stock solutions of PBA, BDBA, and BPBA (10 mM) were initially prepared by dissolving each compound in the MeOH/H_2O solution (4 : 1) and stored at −4 °C. Working solutions at the desired concentrations were then prepared by diluting the stock solutions with the same MeOH/H_2O mixture.

Generation of microdroplets and mass spectrometric analysis

A schematic diagram of the experimental setup for the microdroplet reactions is shown in Fig. 1a. Microdroplets were generated by spraying the solution at a flow rate of 15 μL min^{-1} using a syringe pump, with high-purity nitrogen (90 psi) as the nebulizing gas. This pneumatic nebulization injection method causes the microdroplet surfaces to carry net charges, making the microdroplets overall charged rather than globally neutral.[36–38] The reaction distance, defined as the distance between the tip of the fused silica capillary and the mass spectrometer inlet, was maintained at 15 mm. The inner diameter (I.D.) of the fused silica capillary used for spraying was 75 μm. The products were detected and analyzed using an LTQ-XL mass spectrometer (Thermo-Fisher, Waltham, MA). The inlet capillary temperature of the mass spectrometer was set to 45 °C, with a maximum acquisition time of 100 ms. To prevent in-source fragmentation, the tube lens voltage was maintained at 0 V. Collision-induced dissociation (CID) was employed to examine the structural characteristics of the products. All experiments were conducted under atmospheric pressure.

Density functional theory (DFT) calculations

All calculations were performed using Gaussian 16 with the B3LYP functional and the 6-311+G(d,p) basis set.[11,39] The convergence criteria for geometry optimization were set to 1×10^{-5} hartree for energy changes, 0.00045 hartree $bohr^{-1}$ for maximum forces, and 0.0018 Å for maximum displacements. The SCF convergence threshold was set to 1×10^{-6} hartree. The impact of an oriented external electric field was initially investigated using Gaussian 16, defining the EEF axis, direction, and magnitude with the "field = $M \pm N$" keyword. Frequency calculations were performed to confirm the nature of the minimum (no imaginary frequency) and transition states (one imaginary frequency).[40,41]

Results and discussion

Fig. 1a illustrates the setup of a typical microdroplet experiment, with detailed experimental methods provided in the ESI.† Briefly, phenylboronic acid (PBA) (100 μM) was dissolved in a MeOH/H_2O solution, and N_2 (90 psi) was used as the nebulizing gas. The MeOH/H_2O ratio was optimized to 4 : 1 to enhance the solubility of PBA. The sample solution was introduced into a fused silica capillary at a flow rate of 15 μL min^{-1} using a syringe pump. The chemical components of the microdroplets were subsequently introduced directly into the mass spectrometer and analyzed in negative ion mode. As shown in Fig. 1c, when the microdroplets containing PBA were introduced into the mass spectrometer *via* pneumatic spray, the PBA dimer (*m*/*z* 225.09) and the hydrated dimer (*m*/*z* 243.10) peaks were detected, indicating that PBA can spontaneously dimerize within the microdroplets at room temperature. Additionally, the low signal intensity of the PBA monomer peak (*m*/*z* 121.05) suggests a high efficiency of the dimerization reaction. Fig. 1b shows the proposed reaction scheme for the spontaneous dimerization of PBA within the MeOH/H_2O microdroplets. In order to confirm the chemical nature of the reaction products, tandem mass spectrometry (MS^2) was used to visualize the fragmentation of the products. The MS^2 spectrum of the dimeric parent ion (*m*/*z* 225.09) shown in Fig. 1d revealed a peak at *m*/*z* 121.05, corresponding to a fragment of the PBA monomer. In the MS^2 spectrum of the hydrated dimer (*m*/*z* 243.10) presented in Fig. 1e, we also observed the dehydrated dimer fragment and the PBA monomer fragment, providing additional support for the structure of the product.

To further investigate the role of the gas–liquid interface in microdroplets, we explored the influence of sheath gas pressure on product abundance. As shown in Fig. 1f, the relative

Open Access Article. Published on 04 April 2025. Downloaded on 6/15/2025 9:25:23 PM.
This article is licensed under a Creative Commons Attribution-NonCommercial 3.0 Unported Licence.

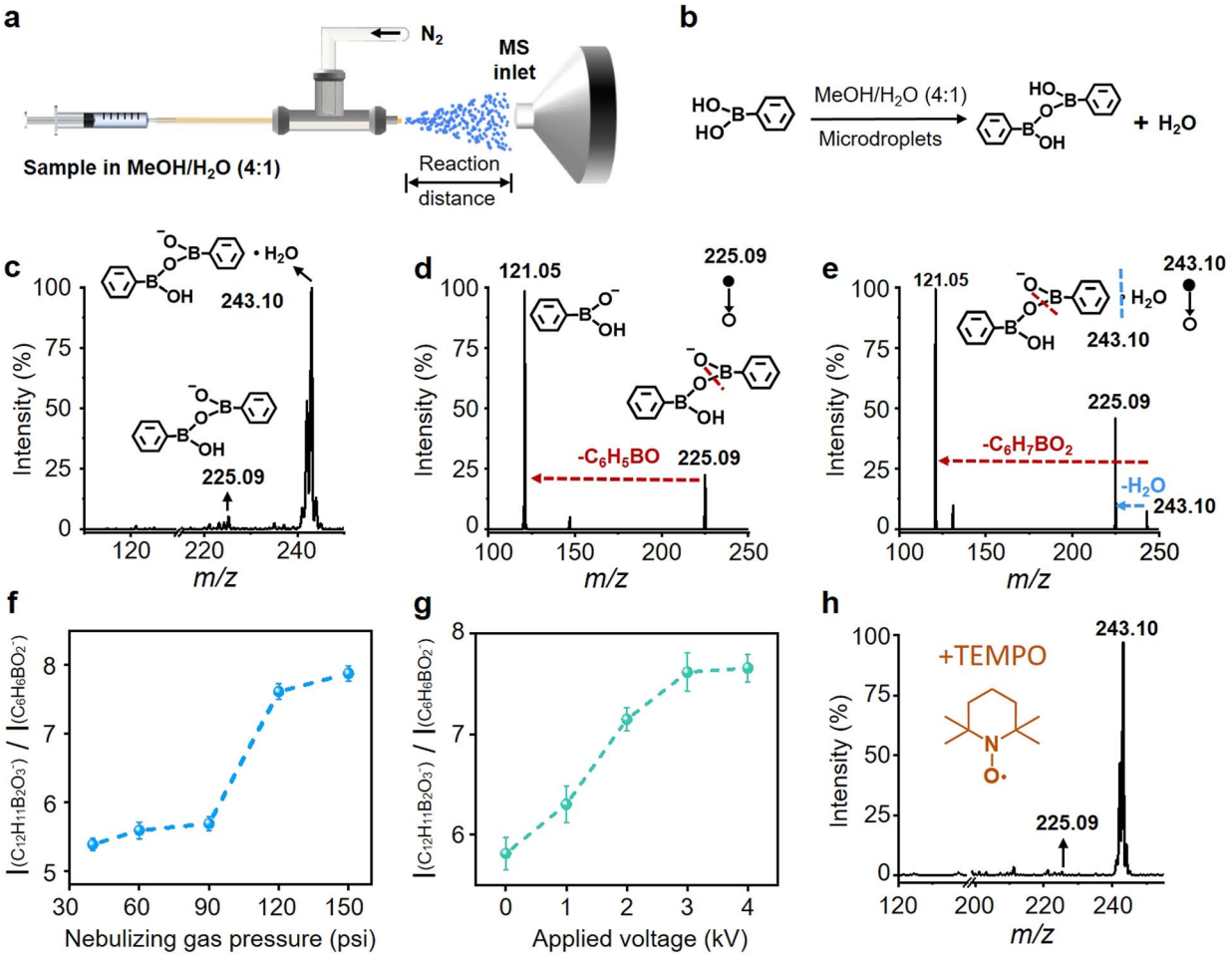

Fig. 1 Spontaneous dimerization of PBA in MeOH/H_2O (4 : 1) microdroplets. (a) Schematic diagram of the experimental setup. (b) Proposed reaction scheme. (c) Mass spectrum of PBA in microdroplets of MeOH/H_2O (4 : 1) using N_2 as the nebulizing gas. (d) MS^2 spectrum of the peak at *m/z* 225.09 shown in panel (c). (e) MS^2 spectrum of the peak of *m/z* at 243.10 shown in panel (c). Intensity ratio of products and reactant as a function of (f) the sheath gas pressure and (g) applied voltage when the reactant concentration is 100 μM and the reaction distance is 15 mm. (h) Mass spectrum of PBA in microdroplets with the addition of TEMPO.

abundance of the PBA dimer products increases gradually as the pressure rises from 40 psi to 150 psi. It is well-established that increasing pressure reduces the size of microdroplets, thereby increasing their specific surface area.[1,14,42] These results highlight the critical role of the gas–liquid interface in facilitating the covalent condensation of PBA.

In addition, according to previous studies,[42–44] a higher electric field at the gas–liquid surface can be obtained by applying a high voltage. We further investigated the effect of interfacial EFs on the PBA condensation process by modulating the applied voltage in the microdroplet system. As shown in Fig. 1g, the relative abundance of the PBA dimer products increases with increasing voltage, suggesting that the interfacial electric field plays a crucial role in facilitating the covalent condensation of PBA.

Considering that the strong electric field at the microdroplet interface can also extract electrons from hydroxide ions (OH^-) in water, producing reactive OH radicals, we explored whether OH radicals affect PBA condensation by introducing the radical scavenger 2,2,6,6-tetramethylpiperidine-1-oxyl (TEMPO) to eliminate OH radicals.

As shown in Fig. 1h, after adding TEMPO in microdroplets, the PBA dimer (*m/z* 225.09) and the hydrated dimer (*m/z* 243.10) peaks are still observed with consistent intensity in the MS spectrum. Such a result indicates that OH radicals are not involved in the covalent condensation of PBA. It has been reported that boronic acids can undergo polymerization at room temperature under an oriented electric field in a scanning tunneling microscope, whereas spontaneous polymerization in solution does not occur even after several days.[4,45–47] In the current system, with a reaction distance of 15 mm, PBA condensation occurs on the microsecond timescale.[42,48] This suggests that the condensation of PBA is more likely driven by the strong electric field within the microdroplets.

Based on the aforementioned observations, we hypothesized that other boronic acid molecules may undergo similar condensation driven by the EFs at the interface of MeOH/H_2O microdroplets.

 © 2025 The Author(s). Published by the Royal Society of Chemistry

Open Access Article. Published on 04 April 2025. Downloaded on 6/15/2025 9:25:23 PM.
This article is licensed under a Creative Commons Attribution-NonCommercial 3.0 Unported Licence.

Therefore, we prepared a 100 μM solution of 4,4′-biphenyldiboronic acid (BPBA) and conducted microdroplet experiments under the same conditions as described above. Upon introducing the BPBA solution into a mass spectrometer *via* pneumatic spray, spontaneous condensation of BPBA into both dimeric and trimeric forms within the microdroplets was observed. As shown in Fig. 2a, the monomer of BPBA was detected, with a peak at *m*/*z* 241.08 corresponding to the deprotonated monomer $[C_{12}H_{11}B_2O_4]^-$. The presence of MeOH in the solvent led to the formation of a MeOH adduct at *m*/*z*

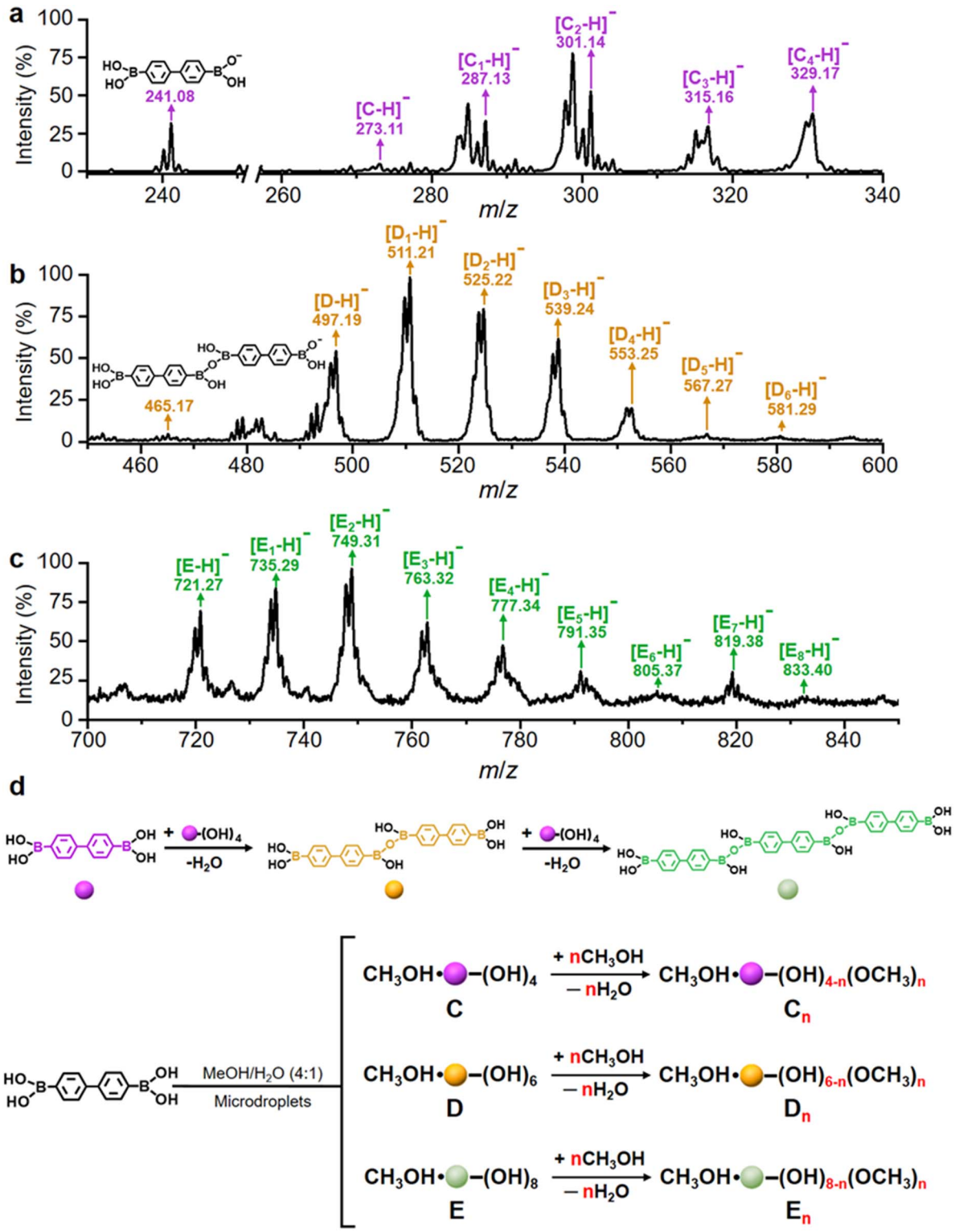

Fig. 2 Spontaneous condensation of BPBA in MeOH/H_2O (4 : 1) microdroplets. (a–c) Mass spectrum of BPBA in microdroplets of MeOH/H_2O (4 : 1) using N_2 as the nebulizing gas with *m*/*z* ranges of 230–340, 450–600 and 700–850. (d) Proposed reaction scheme.

Open Access Article. Published on 04 April 2025. Downloaded on 6/15/2025 9:25:23 PM. This article is licensed under a Creative Commons Attribution-NonCommercial 3.0 Unported Licence.

273.11, represented as $[C_{12}H_{11}B_2O_4 + MeOH]^-$. Additionally, the esterification of the BPBA monomer is also induced by MeOH, yielding the monoester $[C_1–H]^-$ (*m/z* 287.13), diester $[C_2–H]^-$ (*m/z* 301.14), triester $[C_3–H]^-$ (*m/z* 315.16), and tetraester $[C_4–H]^-$ (*m/z* 329.17). The dimerization of BPBA is identified and highlighted in Fig. 2b. The peak at *m/z* 465.17 represents the deprotonated dimer, with the molecular formula $[C_{24}H_{21}B_4O_7]^-$, and the peak at *m/z* 497.19 is attributed to the MeOH adduct of the dimer, with the molecular formula $[C_{24}H_{21}B_4O_7 + MeOH]^-$. Esterification of the dimer with MeOH generated a series of esters, including the monoester $[D_1–H]^-$ (*m/z* 511.21), diester $[D_2–H]^-$ (*m/z* 525.22), triester $[D_3–H]^-$ (*m/z* 539.24), tetraester $[D_4–H]^-$ (*m/z* 553.25), pentaester $[D_5–H]^-$ (*m/z* 567.27), and hexaester $[D_6-H]^-$ (*m/z* 581.29).

Similarly, Fig. 2c reveals the trimerization of BPBA, with a peak at *m/z* 721.27 corresponding to the MeOH adduct of the trimer, $[C_{36}H_{31}B_6O_{10} + MeOH]^-$. Subsequent esterification generated products at *m/z* 735.29 ($[E_1–H]^-$), 749.31 ($[E_2–H]^-$), 763.32 ($[E_3–H]^-$), 777.34 ($[E_4–H]^-$), 791.35 ($[E_5–H]^-$), 805.37 ($[E_6–H]^-$), 819.38 ($[E_7–H]^-$), and 833.40 ($[E_8–H]^-$), representing variously esterified forms ranging from monoester to octaester. The structures of typical products were further confirmed by MS^2, as shown in Fig. S1–S5.† Based on these experimental observations, a reaction scheme is proposed (Fig. 2d), in which BPBA undergoes spontaneous dimerization and trimerization within $MeOH/H_2O$ microdroplets. Both the monomeric and polymeric forms of BPBA participate in esterification reactions with MeOH present in the solvent.

Moreover, a similar room-temperature condensation phenomenon of 1,4-benzenediboronic acid (BDBA) was also observed in $MeOH/H_2O$ microdroplets (Fig. S6†), highlighting the capability of the EFs at the interface of microdroplets to robustly drive the self-condensation of boronic acids.

In addition to the self-condensation of boronic acids, we hypothesized that the strong EFs at the air–liquid interface of microdroplets could also induce co-condensation reactions between different boronic acid molecules. To test our hypothesis, bi-component boronic acid solutions were used as model systems to demonstrate the co-condensation reactions in microdroplets. Fig. 3a shows the mass spectrum of

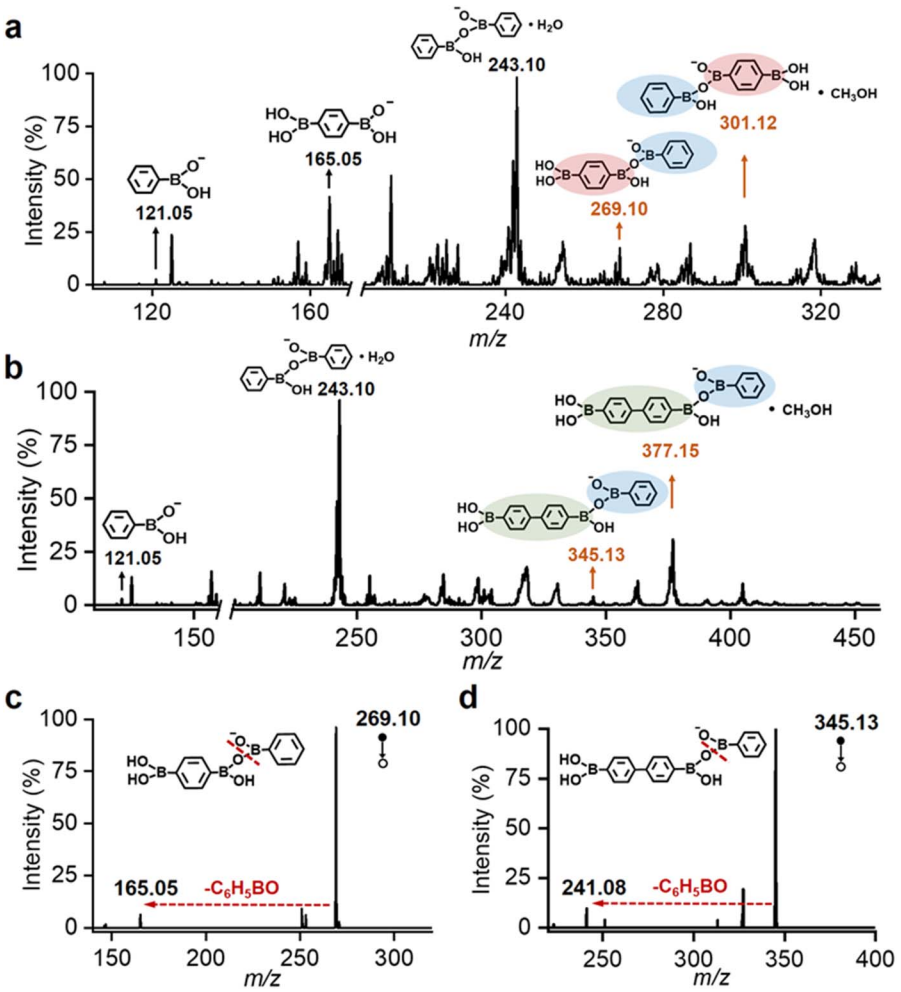

Fig. 3 Spontaneous co-condensation of boronic acids in $MeOH/H_2O$ (4 : 1) microdroplets. Mass spectra of (a) PBA and BDBA and (b) PBA and BPBA in microdroplets using N_2 as the nebulizing gas. (c) MS^2 spectrum of the peak at *m/z* 269.10 shown in panel (a). (d) MS^2 spectrum of the peak at *m/z* 345.13 shown in panel (b).

 © 2025 The Author(s). Published by the Royal Society of Chemistry

Open Access Article. Published on 04 April 2025. Downloaded on 6/15/2025 9:25:23 PM.
This article is licensed under a Creative Commons Attribution-NonCommercial 3.0 Unported Licence.

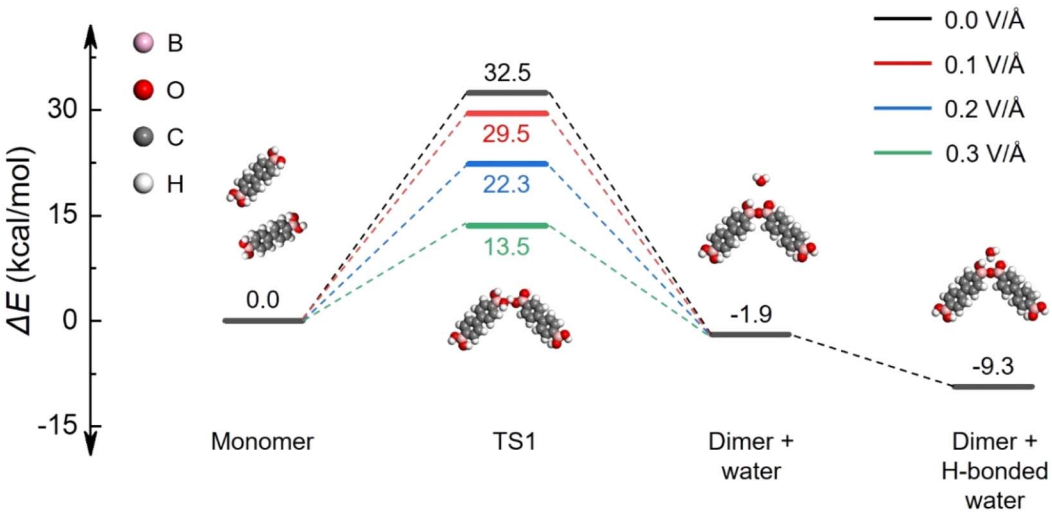

Fig. 4 DFT calculations. The potential energy profile of BPBA condensation in the absence of an external electric field (black trace). Potential energy profile of the transition state under external EFs of 0.1 (red trace), 0.2 (blue trace), and 0.3 V Å^{-1} (green trace). Potential energy profile of the reaction was calculated at the B3LYP/6-311+G(d,p) level of theory.

microdroplets that contained PBA and BDBA. In addition to the characteristic peaks of PBA (m/z 121.05), BDBA (m/z 165.05), and the PBA dimer (m/z 243.10), two new peaks corresponding to PBA–BDBA co-condensation products at m/z 269.10 and 301.01 can also be detected. The MS^2 spectra of these two products shown in Fig. 3c and S11† further revealed the fragments of PBA and BPBA, supporting the formation of PBA–BDBA co-condensation species.

Similarly, for a mixed solution of PBA and BPBA, reactions in the microdroplets yielded peaks at m/z 345.13 and 377.15, attributed to PBA–BPBA co-condensation products (Fig. 3b, d and S12†). These findings indicate that the strong EFs within microdroplets can effectively induce both the self-condensation of boronic acids and cross-coupling reactions between different boronic acid molecules.

In order to understand the role of EFs in the room-temperature condensation of boronic acids, density functional theory (DFT) calculations were performed to reveal the reaction barrier evolution with/without the presence of EFs.[11,39,49] As shown in Fig. 4 and S13,† the activation energy for the formation of the transition state (TS) is substantially reduced by 19.0 kcal mol^{-1} in the presence of EFs (F_z = 0.30 V Å^{-1}) as compared to the TS formation without EFs, indicating that the TS is efficiently stabilized by EFs during the covalent condensation process of BPBA. The potential energy profile shown in Fig. 4 was calculated using the B3LYP functional with the 6-311+G(d,p) basis set, ensuring a reliable description of the reaction energetics.

To further elucidate the influence of EF direction, additional simulations were conducted by applying EFs along different orientations (x-, y-, and z-axes). As shown in Fig. S14,† the EF direction significantly affects the activation energy required for the formation of the TS. As compared to EFs along x- or y-axes, an EF along the z-axis direction yields the greatest reduction in reaction energy barriers, highlighting the specific role of EFs in accelerating the condensation of boronic acids.

Furthermore, simulations of the energy barriers for TS formation under varying EF conditions reveal a progressive decrease in the energy barrier with increasing EF strength. Similar EFs effect was also observed in the simulation results of the PBA condensation system (Fig. S15†). The detailed structural information on the TS under different EF conditions is displayed in Tables S1 and S2,† including charge distributions and bond lengths. These results suggest that strong EFs can markedly promote the covalent condensation of boronic acids. In addition, theoretical calculations were carried out to investigate the impact of external EFs on hydrogen-bonded intermediates, which commonly form between boronic acid oligomers and water during the condensation process.[15] It was found that the hydrogen-bonded complex of the PBA dimer with water can also be stabilized by EFs (Fig. S15†), facilitating the forward reaction during the condensation process. More detailed H-bond behavior under electric fields can be simulated *via* advanced theoretical methods,[50] which is beyond the scope of the present work. These theoretical models further support that the room-temperature condensation of boronic acids can be sufficiently induced by interfacial EFs in MeOH/H_2O microdroplets.

Conclusions

In conclusion, this work provides experimental evidence for the role of EFs in driving the covalent condensation of boronic acids, offering direct insights into electric-field-induced condensation mechanisms. By utilizing the strong EFs at the microdroplet interface, we demonstrate that EFs can effectively facilitate the condensation reaction of boronic acids. This work not only validates the hypothesized role of external EFs in boronic acid chemistry but also introduces a novel solution-phase approach for exploring electric-field effects on condensation reactions. Our findings open up new possibilities for the

Open Access Article. Published on 04 April 2025. Downloaded on 6/15/2025 9:25:23 PM. This article is licensed under a Creative Commons Attribution-NonCommercial 3.0 Unported Licence.

controllable and facile synthesis of highly polymerized materials with unique properties under ambient conditions.

Data availability

The main data supporting the findings of this study are available within the paper and its ESI.† Additional data are available from the corresponding authors upon reasonable request.

Author contributions

Q. L. and Z. F. C. conceived the idea and designed the experiments. Y. W. Z. and M. Y. J. carried out the MS experiments and analyzed the data. The text was initially composed by Y. W. Z., M. Y. J., Q. L. and Z. F. C., and all authors further contributed to the discussion of the experimental work and the final version of the manuscript.

Conflicts of interest

The authors declare no competing interests.

Acknowledgements

Q. L. acknowledges financial support from the Sichuan Science and Technology Program (No. 2025NSFTD0001 and No. 2025ZNSFSC0920) and Sichuan University (No. 2024SCUQJTX007). Z. F. C. acknowledges financial support from the Sichuan Province Science and Technology Project (2024YFHZ0288) and the National Natural Science Foundation of China (Grant No. 22402132). This work was supported by the Fundamental Research Funds for the Central Universities. Jiu-Hong Fang from the Institute of Chemistry, Chinese Academy of Sciences, is thanked for fruitful scientific discussions.

Notes and references

1 D. Zhang, X. Yuan, C. Gong and X. Zhang, *J. Am. Chem. Soc.*, 2022, **144**, 16184–16190.
2 S. Shaik, D. Danovich, J. Joy, Z. Wang and T. Stuyver, *J. Am. Chem. Soc.*, 2020, **142**, 12551–12562.
3 X. Huang, C. Tang, J. Li, L.-C. Chen, J. Zheng, P. Zhang, J. Le, R. Li, X. Li, J. Liu, Y. Yang, J. Shi, Z. Chen, M. Bai, H.-L. Zhang, H. Xia, J. Cheng, Z.-Q. Tian and W. Hong, *Sci. Adv.*, 2019, **5**, eaaw3072.
4 Z.-F. Cai, G. Zhan, L. Daukiya, S. Eyley, W. Thielemans, K. Severin and S. De Feyter, *J. Am. Chem. Soc.*, 2019, **141**, 11404–11408.
5 S. Shaik, D. Mandal and R. Ramanan, *Nat. Chem.*, 2016, **8**, 1091–1098.
6 G. Cassone, J. Sponer and F. Saija, *Top. Catal.*, 2022, **65**, 40–58.
7 S. Shaik, S. P. de Visser and D. Kumar, *J. Am. Chem. Soc.*, 2004, **126**, 11746–11749.
8 G. Cassone, P. V. Giaquinta, F. Saija and A. M. Saitta, *J. Chem. Phys.*, 2015, **142**, 054502.
9 G. Cassone, F. Pietrucci, F. Saija, F. Guyot and A. M. Saitta, *Chem. Sci.*, 2017, **8**, 2329–2336.
10 G. Cassone, A. Sofia, G. Rinaldi and J. Sponer, *J. Phys. Chem. C*, 2019, **123**, 9202–9208.
11 Z. Song, C. Liang, K. Gong, S. Zhao, X. Yuan, X. Zhang and J. Xie, *J. Am. Chem. Soc.*, 2023, **145**, 26003–26008.
12 I. B. Stone, R. L. Starr, N. Hoffmann, X. Wang, A. M. Evans, C. Nuckolls, T. H. Lambert, M. L. Steigerwald, T. C. Berkelbach, X. Roy and L. Venkataraman, *Chem. Sci.*, 2022, **13**, 10798–10805.
13 B. Zhang, C. Schaack, C. R. Prindle, E. A. Vo, M. Aziz, M. L. Steigerwald, T. C. Berkelbach, C. Nuckolls and L. Venkataraman, *Chem. Sci.*, 2023, **14**, 1769–1774.
14 C. Zhu, L. N. Pham, X. Yuan, H. Ouyang, M. L. Coote and X. Zhang, *J. Am. Chem. Soc.*, 2023, **145**, 21207–21212.
15 G. Zhan, Z.-F. Cai, K. Strutyński, L. Yu, N. Herrmann, M. Martínez-Abadía, M. Melle-Franco, A. Mateo-Alonso and S. D. Feyter, *Nature*, 2022, **603**, 835–840.
16 C.-Z. Guan, D. Wang and L.-J. Wan, *Chem. Commun.*, 2012, **48**, 2943–2945.
17 J. F. Dienstmaier, A. M. Gigler, A. J. Goetz, P. Knochel, T. Bein, A. Lyapin, S. Reichlmaier, W. M. Heckl and M. Lackinger, *ACS Nano*, 2011, **5**, 9737–9745.
18 W. L. A. Brooks and B. S. Sumerlin, *Chem. Rev.*, 2016, **116**, 1375–1397.
19 A. P. Côté, A. I. Benin, N. W. Ockwig, M. O'Keeffe, A. J. Matzger and O. M. Yaghi, *Science*, 2005, **310**, 1166–1170.
20 L. Grill and S. Hecht, *Nat. Chem.*, 2020, **12**, 115–130.
21 L. Grossmann, B. T. King, S. Reichlmaier, N. Hartmann, J. Rosen, W. M. Heckl, J. Björk and M. Lackinger, *Nat. Chem.*, 2021, **13**, 730–736.
22 Z.-F. Cai, T. Chen and D. Wang, *J. Phys. Chem. Lett.*, 2023, **14**, 2463–2472.
23 M. Lackinger, *Nature*, 2019, **572**, 448–449.
24 L. Qiu and R. G. Cooks, *Angew. Chem., Int. Ed.*, 2024, **63**, e202400118.
25 J. K. Lee, D. Samanta, H. G. Nam and R. N. Zare, *Nat. Commun.*, 2018, **9**, 1562.
26 Z. Song, C. Zhu, K. Gong, R. Wang, J. Zhang, S. Zhao, Z. Li, X. Zhang and J. Xie, *J. Am. Chem. Soc.*, 2024, **146**, 10963–10972.
27 S. Jin, H. Chen, X. Yuan, D. Xing, R. Wang, L. Zhao, D. Zhang, C. Gong, C. Zhu, X. Gao, Y. Chen and X. Zhang, *JACS Au*, 2023, **3**, 1563–1571.
28 C. F. Chamberlayne and R. N. Zare, *J. Chem. Phys.*, 2020, **152**, 184702.
29 H. X. Hao, I. Leven and T. Head-Gordon, *Nat. Commun.*, 2022, **13**, 280.
30 K. Gong, A. Nandy, Z. Song, Q.-S. Li, A. Hassanali, G. Cassone, S. Banerjee and J. Xie, *J. Am. Chem. Soc.*, 2024, **146**, 31585–31596.
31 M. A. Eatoo, N. Wehbe, N. Kharbatia, X. Guo and H. Mishra, *Chem. Sci.*, 2025, **16**, 1115–1125.
32 X. Li, X. Nong, C. Zhu, X. Gao, H. Chen, X. Yuan, D. Xing, L. Liu, C. Liang, D. Zang and X. Zhang, *J. Am. Chem. Soc.*, 2024, **146**, 29267–29271.

 © 2025 The Author(s). Published by the Royal Society of Chemistry

Open Access Article. Published on 04 April 2025. Downloaded on 6/15/2025 9:25:23 PM.
This article is licensed under a Creative Commons Attribution-NonCommercial 3.0 Unported Licence.

33 L. E. Krushinski, P. J. Herchenbach and J. E. Dick, *Proc. Natl. Acad. Sci. U. S. A.*, 2024, **121**, e2416353121.
34 D. Xing, Y. Meng, X. Yuan, S. Jin, X. Song, R. N. Zare and X. Zhang, *Angew. Chem., Int. Ed.*, 2022, **61**, e202207587.
35 J. K. Lee, K. L. Walker, H. S. Han, J. Kang, F. B. Prinz, R. M. Waymouth, H. G. Nam and R. N. Zare, *Proc. Natl. Acad. Sci. U. S. A.*, 2019, **116**, 19294–19298.
36 H. Q. Xiong, J. K. Lee, R. N. Zare and W. Min, *J. Phys. Chem. Lett.*, 2020, **11**, 7423–7428.
37 Y. Xia, J. Xu, J. Li, B. Chen, Y. Dai and R. N. Zare, *J. Phys. Chem. A*, 2024, **128**, 5684–5690.
38 J. P. Heindel, H. Hao, R. A. LaCour and T. Head-Gordon, *J. Phys. Chem. Lett.*, 2022, **13**, 10035–10041.
39 L. Xue, W. Chen, P. Zheng, J. Geng, F. Zhang, X. Li, Z. Zhang and X. Hu, *J. Am. Chem. Soc.*, 2024, **146**, 26909–26915.
40 P. J. Stephens, F. J. Devlin, C. F. Chabalowski and M. J. Frisch, *J. Phys. Chem.*, 1994, **98**, 11623–11627.
41 S. Wei, Q. Wan, S. Zhou, W. Nie and S. Chen, *J. Am. Chem. Soc.*, 2024, **146**, 32777–32784.
42 Y.-H. Lai, S. Sathyamoorthi, R. M. Bain and R. N. Zare, *J. Am. Soc. Mass Spectrom.*, 2018, **29**, 1036–1043.
43 Y. Meng, R. N. Zare and E. Gnanamani, *J. Am. Chem. Soc.*, 2023, **145**, 19202–19206.
44 Y. Meng, E. Gnanamani and R. N. Zare, *J. Am. Chem. Soc.*, 2023, **145**, 32–36.
45 G. Zhan, Z.-F. Cai, M. Martínez-Abadía, A. Mateo-Alonso and S. De Feyter, *J. Am. Chem. Soc.*, 2020, **142**, 5964–5968.
46 Z. Fu, N. Arisnabarreta, K. S. Mali and S. De Feyter, *Commun. Chem.*, 2024, **7**, 106.
47 Q. Liang, G. Feng, H. Ni, Y. Song, X. Zhang, S. Lei and W. Hu, *Chin. Chem. Lett.*, 2023, **34**, 108006.
48 J. K. Lee, S. Kim, H. G. Nam and R. N. Zare, *Proc. Natl. Acad. Sci. U. S. A.*, 2015, **112**, 3898–3903.
49 G. Cassone, J. Sponer, J. E. Sponer, F. Pietrucci, A. M. Saitta and F. Saija, *Chem. Commun.*, 2018, **54**, 3211–3214.
50 M. F. Torre, A. Amadeo, G. Cassone, M. Tommasini, K. Mráziková and F. Saija, *J. Phys. Chem. A*, 2024, **128**, 5490–5499.